Electronic shell structure and carrier dynamics of high aspect ratio InP single quantum dots

Gareth J. Beirne,[1] Matthias Reischle,[1] Robert Roßbach,[1] Wolfgang-Michael Schulz,[1] Michael Jetter,[1] Jan Seebeck,[2] Paul Gartner,[2,3] Christopher Gies,[2] Frank Jahnke,[2] and Peter Michler[1]

[1]*Institut für Halbleiteroptik und Funktionelle Grenzflächen, Universität Stuttgart, Allmandring 3, 70569 Stuttgart, Germany*

[2]*Institut für Theoretische Physik, Universität Bremen, 28334 Bremen, Germany*

[3]*National Institute for Materials Physics, POB MG-7, Bucharest-Magurele, Romania*

(Received 14 December 2006; published 3 May 2007)

Systematic excitation-power-density dependent and time-resolved single-dot photoluminescence studies have been performed on type-I InP/$Ga_{0.51}In_{0.49}P$ quantum dots. These dots are rather flat and therefore exhibit larger than normal single-dot ground-state transition energies ranging from 1.791 to 1.873 eV. As a result of their low height, the dots have a very high aspect ratio (ratio of width to height) of approximately 27:1. In general, even at high excitation power densities, the dots with ground-state transition energies above 1.82 eV exhibit only *s*-shell emission, while the larger dots exhibiting ground-state emission below 1.82 eV tend to exhibit emission from several (in some cases up to eight) shells. Calculations indicate that this change is due to the smaller dots having only one confined election level while the larger dots have two or more. Time-resolved investigations indicate the presence of fast carrier relaxation and recombination processes for both dot types, however, only the larger dots display clear interlevel relaxation effects as expected. The temporal behavior has been qualitatively simulated using a rate equation model. Also, in a more detailed analysis, the fast carrier relaxation is described on the basis of a quantum kinetic treatment of the carrier-phonon interaction. Finally, the dots display a clear single-photon emission signature in photon statistics measurements.

DOI: 10.1103/PhysRevB.75.195302 PACS number(s): 78.67.Hc, 73.21.La

I. INTRODUCTION

Quantum dots (QDs) possess a discrete density of states and are therefore often referred to as tailored atoms as, unlike real atoms, their electronic and optical properties can be tuned over a large range of values.[1] QDs that have a high aspect ratio are the topic of this paper. Such QDs are interesting as they allow for a significant tuning of the electronic interlevel spacing within the QDs without significantly shifting the associated QD ground-state emission energy. This property is advantageous for applications where one requires a QD with a tailored electronic structure to emit within a specific wavelength range.

Another advantage of QDs with high aspect ratios is that they can be produced with relatively large lateral sizes without the formation of dislocations. This characteristic is important as recent work has shown that enlarged QDs offer advantages with respect to certain applications in the fields of quantum information science. For example, for a particular material system, larger QDs possess an enhanced excitonic oscillator strength when compared to smaller ones. Consequently, such dots have helped to enable the realization of strong coupling in solid-state cavity quantum electrodynamics.[2]

A number of works have studied InP/$Ga_xIn_{1-x}P$ QDs at the single-dot level,[3–7] for example, Zwiller *et al.* have reported single-photon emission from InP/$Ga_xIn_{1-x}P$ QDs emitting at approximately 1.80 eV.[5] In this work, we systematically examine the photoluminescence (PL) emission from similar single InP/$Ga_{0.51}In_{0.49}P$ QDs that have a high aspect ratio of approximately 27:1, as a function of the QD emission energy and consequently as a function of the range of QD energy level spacings provided by the QD ensemble. We show that the QDs (labeled QD2 for convenience) that emit on the low-energy side of the ensemble generally tend to have small energy level spacings as a result of their relatively large lateral size. Therefore, such dots tend to exhibit pronounced state filling effects and complex carrier dynamics involving several shells. On the other hand, the QDs (labeled QD1) that emit on the high-energy side of the ensemble tend to exhibit only ground-state (*s*-shell) emission.

II. EXPERIMENT

The samples were grown by metal-organic vapor phase epitaxy on a (100) GaAs substrate oriented by 6° toward the [111]*A* direction. A 430 nm $Ga_xIn_{1-x}P$ barrier layer was deposited at 720 °C following the deposition of a 300 nm GaAs buffer layer at 750 °C directly onto the substrate. The QDs were then produced by depositing two monolayers of InP material at 710 °C. The samples used for PL were overgrown at 710 °C by a 30 nm GaInP capping (barrier) layer. Mesas with a diameter of 200 nm were then fabricated by electron-beam lithography and dry etching in order to enable the isolation of single QDs that could be identified through their optical-emission spectra and photon statistics properties.

In order to perform micro-PL experiments at 4 K, the samples were mounted in a He-flow cryostat which could be scanned both horizontally and vertically using two stepper motors each with an effective spatial resolution of 50 nm. The single QDs were nonresonantly excited using a frequency-doubled, tunable Ti:sapphire laser emitting 100 fs pulses at 410 nm (3.024 eV) with a repetition rate of 76.2 MHz (13.12 ns between successive pulses). The light to and from the sample was transmitted through a 50× microscope objective which could focus the laser emission down to a spot diameter of approximately 1 μm using a piezo-based actuator. The resulting PL was dispersed using a 0.75 m spectrometer and detected (1) using a liquid-nitrogen-cooled charge-coupled-device camera when taking

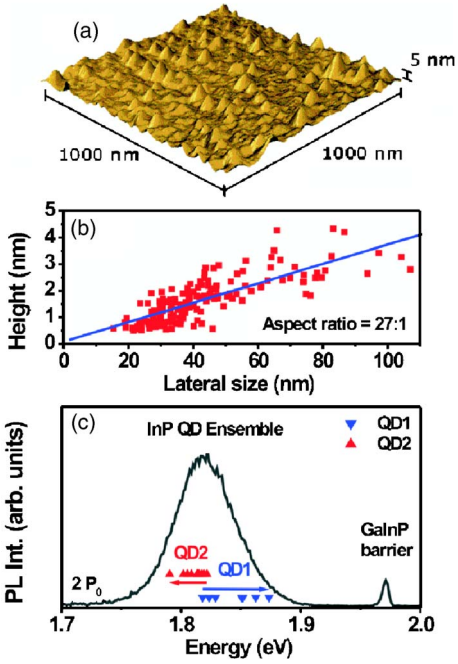

FIG. 1. (Color online) (a) 1 μm^2 AFM image of uncapped InP QDs grown using the same growth parameters that were used to produce the capped QDs. Please note that the height dimension of the image is highly magnified with respect to the lateral dimensions. (b) QD height versus lateral size for the uncapped QDs. The line through the data points is a linear fit to the data and has a slope of 0.037 (1/27). This implies that the average aspect ratio is 27:1. In other words, for a 1 nm change in QD height there is an associated 27 nm change in the QD lateral dimensions. (c) QD ensemble PL emission spectrum from nominally identical capped QDs recorded at 4 K and an excitation power density of 4 W/cm^2 ($2P_0$). The markers indicate the GS (biexciton) emission energy of the 18 single QDs that have been investigated to date.

spectra, (2) using two avalanche photodiodes (APDs), one in each path of a Hanbury-Brown and Twiss setup, when performing autocorrelation measurements,[8] and (3) using an APD with a high temporal resolution when recording time-resolved PL measurements using the time-correlated single-photon-counting technique. PL rise times and decay times as low as 35 ps could be reliably measured using this setup.

III. RESULTS AND DISCUSSION

A. Structural characterization

Atomic force microscopy images [see Fig. 1(a)] indicate that the QDs on uncapped samples have (a) an average height of 1.7±0.8 nm, a value that accounts for their relatively high PL emission energy of approximately 1.82 eV (680 nm), (b) an average lateral extent of 43±18 nm, (c) an average aspect ratio of 27:1, and (d) a sample surface density of approximately 1.6×10^{10} cm^{-2} [Fig. 1(b)]. Please note that a bimodal QD size distribution (QD1 and QD2) is not observed structurally and that such labeling is simply used to more clearly explain the single-dot PL results presented later. As shown in Fig. 1(b), the dots actually exhibit a unimodal size distribution. This implies that the dramatic change of the dot optical properties across the ensemble is probably related to the rapid but nonetheless continuous change of lateral QD size and does not result from a sudden size transition. It is also clear from Fig. 1(b) that it is possible to observe QD1-type dots on the QD2 side of the ensemble, and vice versa; however, as we have found such observations are relatively unlikely.

B. Single-dot photoluminescence

To date, 18 single QDs have been examined in detail, namely, eleven QD2 and seven QD1 dots. The investigated dots span the QD ensemble emission range which is centered at 1.8199 eV with a full width at half maximum (FWHM) of 49.8 meV, and the ground-state emission energy of each is indicated by a triangular marker in Fig. 1(c). Remarkably, to date, using these growth conditions, we have not observed a QD2 dot exhibiting ground-state (GS) related biexciton emission above 1.822 eV (QD2 biexciton observed from 1.7905 to 1.8217 eV=31.2 meV range), or a QD1 dot exhibiting GS biexcitonic emission below 1.818 eV (QD1 biexciton observed from 1.818 to 1.8734 eV=55.4 meV range). This observation indicates that the QD lateral size varies rapidly as a function of the QD GS transition energy as expected for high aspect ratio QDs.

PL features arising from the barrier and the wetting layer (WL) have also been observed. In Fig. 1(c), the $Ga_xIn_{1-x}P$ barrier emission is clearly observed at approximately 1.973 eV. This implies that the total (conduction band plus valence band) QD1 GS offset is typically less than 150 meV, while the associated value for QD2 is typically greater than this value. Clear WL emission, centered at 1.928 eV, has been observed in micro-PL measurements (not shown). We estimate that this implies that the WL is approximately equivalent to a 1.5 monolayer thick $InP/Ga_{0.51}In_{0.49}P$ quantum well layer.

In Fig. 2(a) we present QD1 (QD2) single-dot PL spectra recorded as a function of excitation power density (PD). At a PD of 2 W/cm^2 (P_0), the QD1 (QD2) PL spectrum displays two emission lines. The higher-energy peak labeled *X*, observed at 1.8333 eV (1.8187 eV) with a FWHM of 0.71 meV (0.62 meV), displays a linear increase of integrated PL intensity with PD indicating excitonic character. On the other hand, the second, initially less intense, peak labeled *XX* observed at 1.8291 eV (1.8133 eV) with a FWHM of 1.23 meV (0.50 meV), and located 4.2 meV (5.4 meV) below *X*, as a result of the biexciton binding energy, shows a superlinear (almost quadratic) power dependence indicating biexcitonic character. At a PD of $10P_0$, the *XX* line of both QD1 and QD2 dominates both spectra, whereas the *X* line is found to diminish rapidly with increasing PD.

In the case of QD1, further increases in illumination only lead to a saturation of the related *XX* emission, while in contrast, for QD2, intense *p*-shell emission, located, in this case, 10.4 meV above the *XX* (*s*-shell) line, starts to rapidly emerge. At successively higher PDs, further higher-energy peaks originating from ever higher-lying levels appear. The

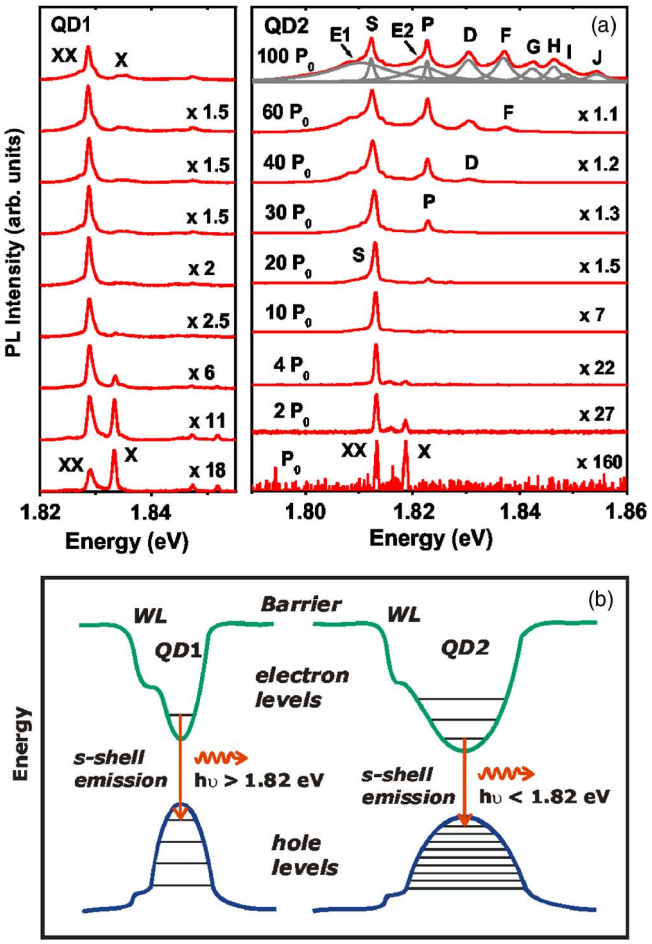

FIG. 2. (Color online) (a) PL spectra recorded at 4 K as a function of PD from QD1 (left graph) and QD2 (right graph). At low PDs both sets of spectra display clear excitonic emission features, namely, an exciton and a biexciton, however, at high PDs QD2 also displays a clear shell structure, whereas no such structure is apparent from QD1. At $100P_0$, a good fit of the QD2 PL spectrum may be achieved using ten Lorentzian peaks. (b) Schematic illustration of the proposed band structure of QD1 and QD2, with the former proposed to have only one confined electron shell while the latter is proposed to have several. Please note that the schematic drawing is intended to sketch the confinement situation and the resulting states without referring to the spatial directions. The interlevel energy spacing for both electrons and holes depends primarily on the lateral size of the quantum dot in question while the wetting layer and barrier states are defined along the growth direction.

observation of PL emission from such states in QD2 indicates that the electrons and holes have already filled all of the previously available lower-lying states. The absence of such emission in the corresponding QD1 PL spectra indicates that either the electron or the hole excited states are not confined in this case. The lack of such states is thought to be due to the smaller height, and therefore to the significantly smaller lateral dimensions of these dots, with the latter in turn leading to a larger electron (and hole) interlevel spacing. Taking into account the considerably smaller effective mass of the electrons, this implies that QD1 may only have one bound electron level. Further evidence for this proposal is provided by the absence of clear multiexcitonic states, such as triexcitons and higher-order excitons, in the QD1 PL spectra, as these complexes would require the presence of a bound *p*-shell for both the electrons and the holes. In contrast, intense PL emission from such complexes is readily observed on the low-energy side of the QD2 *XX* [labeled *E*1 in Fig. 2(a)] in agreement with this hypothesis.

TABLE I. Fitting parameters for the ten Lorentzian peaks required to attain a good fit of the $100P_0$ QD2 PL spectrum presented in Fig. 2(a).

No.	Label	Energy (eV)	ΔE (meV)	FWHM (meV)
1	*E*1	1.81017	*S* (*XX*)−2.1	13.21
2	*S* (*XX*)	1.81227	0	1.21
3	*E*2	1.82198	*S*+9.71	7.81
4	*P*	1.82268	*S*+10.41	0.93
5	*D*	1.83044	*P*+7.76	3.87
6	*F*	1.83696	*D*+6.52	3.64
7	*G*	1.84235	*F*+5.39	3.55
8	*H*	1.84639	*G*+4.04	2.94
9	*I*	1.84869	*H*+2.30	3.44
10	*J*	1.85432	*I*+5.63	4.07

The shell structure of QD2 observed via PL at $100P_0$ is to our knowledge the most detailed reported to date from a single QD,[9–12] [right topmost spectrum in Fig. 2(a)]. An accurate fit of this data can be achieved using ten Lorentzian functions, the associated fit parameters of which are listed in Table I. Not counting the broad shoulders, labeled *E*1 and *E*2, on the low-energy side of both the *s*-shell and the *p*-shell, at least eight distinct peaks can be observed. The first three features may be relatively unambiguously identified as emission from the *s* (GS), *p*, and *d* shells, and are consequently labeled *S*, *P*, and *D*, respectively. The five remaining higher-energy peaks have not been reliably identified to date and are therefore tentatively labeled *F*, *G*, *H*, *I*, and *J*. The two broad PL features *E*1 and *E*2 observed at high PDs [Fig. 2(a) and Table I] are thought to be due to the recombination of various higher-order excitons that spectrally overlap as a result of the complicated interaction that occurs between such complexes when the QD is occupied by large numbers of carriers. Excitonic effects are also thought to be the primary reason for the relatively broad FWHM (3–4 meV) of the *D*, *F*, *G*, *H*, *I*, and *J* peaks (see Table I). Please note that the majority of QD2 dots exhibit PL emission from a smaller number of shells.

C. Energy level calculations

The $InP/Ga_{0.51}In_{0.49}P$ valence-band offset is negative in the absence of strain, i.e., type-II, with the InP valence band 45 meV below that of $Ga_{0.51}In_{0.49}P$.[13] This implies that the holes are forced to remain in the barrier and are not confined by the QDs. The situation changes dramatically, however, if one takes into account the strong strain fields that are invariably present in and around self-assembled QDs. This strain distribution is generally inhomogeneous and anisotropic. The

hydrostatic component of the strain strongly shifts both the conduction- and valence-band edges, while the biaxial component further modifies the valence band by lifting the light- and heavy-hole degeneracy, with the heavy hole shifted to higher energies and the light hole shifted to lower energies.[14] Consequently, the heavy-hole band offset is expected to become strongly positive for dots that have a sufficiently large diameter and low height, i.e., for dots that have a high aspect ratio. Subsequently, the heavy holes are predicted to become strongly confined to the center of such QDs. In contrast, the light holes become even more type-II and continue to remain outside the dots. If, however, the dot height is strongly increased, the strain will eventually become too low to confine the heavy hole to the dot center, and it will be forced to reside at the radial boundary outside the dot as for the unstrained case. In previous work, we have found that this type-II to type-I transition occurs somewhere between dot heights of 20 and 5 nm.[7]

A reliable calculation of the localized hole states is difficult due to the complexity of the confinement situation.[13] Therefore, we restrict ourselves to an estimation of the number of bound QD states for electrons. Given the high aspect ratio of the dots, the dependence of the height z on the radial coordinate ρ is smooth. This is exactly the requirement for the applicability of the adiabatic approximation,[15] which allows for a decoupling of the z motion from the in-plane motion. In this approximation, z is the "fast-moving coordinate" and the energy of the ground-state solution of the motion in the z direction at a given position ρ acts as a potential for the "slow" ρ motion. Obviously, this potential has a minimum at the QD center and therefore may give rise to localized states. By using a GS offset of 150 meV or smaller for QDs with a height of 1.2 nm (QD1), one obtains only one bound electron state. On the contrary, for a height of 2.4 nm (QD2) using the same offset one obtains five electron shells with an energy spacing of about 8.5 meV. In fact, as mentioned above, the offset for QD2 is larger, since for larger dots the strain is lower, and this should in turn lead to an even higher number of bound shells. Assuming that the number of localized hole states is larger due to their larger effective mass, the number of PL lines should be controlled by the number of bound electron states. A schematic illustration of the proposed band structure of QD1 and QD2 is presented in Fig. 2(b). The key message is that QD1 is expected to only contain one confined electron shell, while QD2 should contain two or more.

D. Time-resolved single-dot photoluminescence

Time-resolved single-dot PL measurements have been performed as a function of PD in order to examine the carrier dynamics of the two dot types. The results for the QD1, X and XX (S), and the QD2, XX (S), P and D emission lines, are presented in Fig. 3. In general, all of the transients show a fast rising edge and a nonexponential decay. However, in the case of QD2 each of the transients shows an increasingly delayed PL intensity maximum with increasing PD. For a specified PD, the estimated time at which this maximum occurs is listed for each peak in Table II with increasing PD.

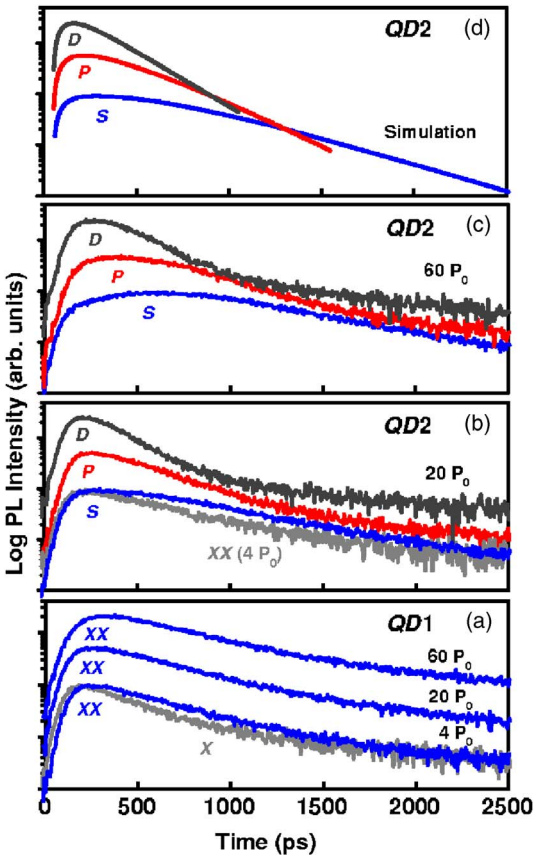

FIG. 3. (Color online) (a) PL intensity versus time taken at 4 K for both the X and XX emission of QD1 at different PDs. (b) PL intensity versus time for the S (XX), P, and D emission from QD2 recorded at moderate PDs, and (c) the S, P, and D emission from QD2 taken at $60P_0$. The delay of the maximum peak intensities at high PDs is thought to be due to delayed filling from higher-lying levels. (d) Curves generated using Eq. (1) which closely reproduce the related $60P_0$ data for the investigated shells. Where necessary the curves have been shifted vertically for clarity.

This maximum, which is followed by a power-independent PL decay, is thought to originate from delayed pumping of lower-lying levels by occupied higher levels. In contrast, the clear absence of such cascaded emission processes in the PL transients of QD1, once again, suggests that only one electron level is confined in QD1.

The QD1 and QD2 (not shown) X decay times are fast at approximately 350 and 450 ps at 4 P_0, respectively, and closely match the estimated atomic-like radiative lifetime of

TABLE II. Estimated time at which the QD1 XX and the QD2 S, P, and D PL emission lines reach a maximum at various PDs.

	QD1	QD2		
PD (units of P_0)	XX (ps)	S (XX) (ps)	P (ps)	D (ps)
4	230	200		
20	240	250	230	200
60	310	560	400	260

approximately 350 ps, calculated by assuming a maximum electron-hole wave function overlap.[16] This clearly implies that QD1 and QD2 have a type-I electronic alignment with heavy holes strongly confined within the dot. From a simple statistical point of view, one would normally expect the *XX* lifetime to be half that of the associated *X*; however, this is clearly not the case, as the decay time of the QD1 and the QD2 XX PL lines at 4 P_0 are approximately 480 ps [Fig. 3(a)] and 580 ps [Fig. 3(b)]. Deviations from the expected ratio have also been reported for other QD material systems[17] and have been predicted[18,19] when the different spatial wave function distribution, spin structure, and coupling to the photon field of excitons and biexcitons were taken into account.[20]

E. Rate equation model

We have used a rate equation model to simulate the temporal behavior of QD2,[11] and have considered the situation at low PDs where only the *S* ($l=1$), *P* ($l=2$), and *D* ($l=3$) lines would be observed in PL spectra. The model assumes (1) that state filling effects and cascaded relaxation via neighboring energy levels dominate the carrier dynamics, (2) that carrier capture into each state from higher-lying QD states ($l \geq 4$) and from WL and barrier states occurs, and (3) that the state occupation decays exponentially. Using this approach, the following relation was used to simulate the temporal evolution of the state occupation:

$$\frac{dN_l}{dt} = -\tau_l^{-1} N_l - \tau_{l-1l}^{-1} N_l (1 - N_{l-1}) + \tau_l^{-1}{}_{l+1} N_{l+1} (1 - N_l) + \tau_{lHS}^{-1} N_{HS} (1 - N_l) \quad (1)$$

where $l=1,2,3$; N_l and τ_l^{-1} are the occupation rate and recombination rate of the state l, respectively, τ_{kl}^{-1} is the interlevel relaxation rate between the states k and l, and the subscript *HS* represents higher-lying states. The results of the simulation are found to qualitatively describe the temporal behavior of QD2 and are presented in Fig. 3(d). The values used for the initial occupation rate of each state were $N_{HS}=0.3$, and $N_3=N_2=N_1=0$, and the optimum fitting parameters were found to be $\tau_1=420$ ps, $\tau_2=2000$ ps, $\tau_3=1500$ ps, $\tau_{12}=340$ ps, $\tau_{23}=180$ ps, $\tau_{3HS}=300$ ps, $\tau_{2HS}=530$ ps, and $\tau_{1HS}=700$ ps.

F. Quantum kinetic calculations

To gain a deeper insight into the physical processes connected with the observed luminescence dynamics, we also apply a more refined microscopic treatment which combines a description of carrier relaxation dynamics on a picosecond time scale with a description of carrier recombination dynamics on a nanosecond time scale. For this purpose, we use a kinetic equation,

$$\frac{d}{dt} f_\alpha^a = \left.\frac{d}{dt} f_\alpha^a\right|_{spont} + \left.\frac{d}{dt} f_\alpha^a\right|_{phon}, \quad (2)$$

where f_α^a is the population of state α with $a=e,h$ for electrons and holes, respectively. Carrier relaxation is described within a (nonperturbative) quantum kinetic theory for the carrier–LO-phonon interaction including polaron and memory effects as well as the coupling of QDs to the WL.[21]

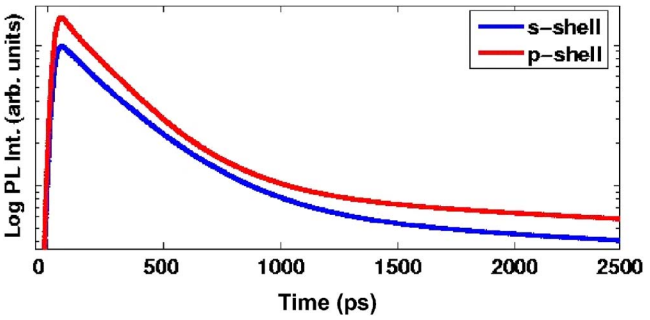

FIG. 4. (Color online) Calculation using Eq. (2) of the temporal evolution of the *s*-shell and the *p*-shell PL signals from InP dots at 10 K following the excitation of carriers in the wetting layer. To mimic the finite temporal resolution of the experiment, a convolution of the theoretical result with a Gaussian (FWHM=35 ps) was performed. Please note that for better visibility the PL signal for the *p*-shell has been shifted vertically.

Within the microscopic analysis it is presently not feasible to calculate the carrier scattering and luminescence dynamics for a QD system with a large number of confined shells, as observed in the experiments outlined above. Hence, we restrict ourselves to a simpler system with confined *s* and *p* shells and WL states for electrons and holes. The level spacing is chosen in such a way that for low-density excitation conditions a phonon bottleneck for the scattering to the lowest confined electron state is predicted by perturbation theory. It turns out that the results from the microscopic analysis depend only weakly on the exact values used for the level spacing. In the example below, we chose 34.4 meV for electrons and 9.6 meV for holes, whereas the LO-phonon energy is 46 meV.

Considering the case of pulsed optical excitation of the WL states, but in the first step neglecting carrier recombination, we also find efficient carrier relaxation for the present low-temperature conditions, in contradiction to the results from perturbation theory. From the quantum kinetic calculation we find that the evolution toward a steady-state population can be approximately described by a relaxation time of $\tau^e=3.5$ ps for electrons and $\tau^h=1.5$ ps for holes. These relaxation times are effective values, considering all of the possible inward and outward scattering processes. In the second step, the relaxation-time approximation with the aforementioned time constants is combined with a microscopic theory for the PL of semiconductor QDs.[22] The relaxation-time approximation is justified in this case by the clear separation of the time scales required for relaxation and recombination. Please note that for elevated excitation densities carrier-carrier scattering (Auger-like processes) should also contribute to fast scattering processes, while at low carrier densities the polaron processes discussed above are expected to dominate.

The luminescence dynamics calculated according to the theory outlined in Ref. 22 are shown in Fig. 4. The results of the calculation have been convoluted with a Gaussian of the experimental time resolution. First, due to fast carrier relax-

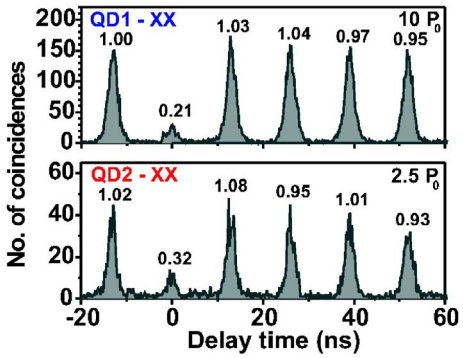

FIG. 5. (Color online) QD1 and QD2 *XX* autocorrelation measurements recorded at moderate PDs (upper and lower graphs, respectively). Both graphs display the unambiguous signature of single-photon emission, thereby implying that the source of the emission in each case is a single QD.

ation, a fast rise of the PL intensity is observed. From our quantum kinetic calculation we find practically the same relaxation time for the *s* and the *p* shell, and therefore, as observed, similar rise times are expected in the PL signal. For later times, when the QD is populated, the decay of the PL intensity is governed by spontaneous recombination. Initially, the decay of the PL signal from the *p*-shell is faster, because, in addition to recombination, carrier relaxation to the *s*-shell further reduces the *p*-shell population. At longer delay times, the decay of the PL signal reveals a nonexponential signature. As discussed in Ref. 22, this is due to the fact that the electrons and holes are not fully correlated. In addition, the carrier redistribution between *s* and *p* shell contributes to the observed time evolution.

G. Second-order autocorrelation

Finally, pulsed second-order autocorrelation measurements $[g^{(2)}(\tau)]$ of the intense QD1 and QD2 *XX* emission lines have been performed in order to prove the zero-dimensional nature of both dot types, and the results are presented in Fig. 5. The area of the coincidence peak at $\tau=0$ is equivalent to 21% and 32% of the Poisson-normalized level calculated from the coincidence data of QD1 and QD2, respectively. This indicates a decrease in multiphoton emission pulses by a factor of approximately 5 for QD1 and 3 for QD2 when compared to a Poissonian source of the same average intensity. This observation in turn indicates that these high aspect ratio QDs are capable of providing triggered single-photon emission and are therefore zero dimensional in nature.

IV. CONCLUSIONS

In conclusion, we have systematically examined high aspect ratio (27:1) $InP/Ga_xIn_{1-x}P$ QDs across the associated QD ensemble emission range. The power-dependent PL measurements reveal a strikingly different behavior on each side of the ensemble. In general, even at high PDs, the dots with GS emission above approximately 1.82 eV exhibit only *s*-shell emission, while the larger dots with GS emission below 1.82 eV tend to exhibit emission from several shells. Calculations show that the rapid change of PL properties as a function of ground state emission energy is due to the smaller QD1 dots having only one confined electron level, while the larger QD2 dots have at least two confined electron levels. Time-resolved PL studies and a rate equation model show that interlevel carrier relaxation processes are observable only in the QD2 PL transients; an observation consistent with the time-integrated PL measurements. In addition, the fast carrier relaxation has been described using a quantum kinetic theory for the carrier-phonon interaction. Finally, using photon statistics measurements, we have confirmed the zero-dimensional nature of both the QD1 and the QD2 dots.

ACKNOWLEDGMENTS

The Stuttgart group acknowledges financial support from the Alexander von Humboldt Foundation. The Bremen group acknowledges financial support from the Deutsche Forschungsgemeinschaft and a grant for central processing unit (CPU) time at the John von Neumann Institute for Computing (NIC), Forschungszentrum Jülich.

[1] For an overview see *Single Quantum Dots*, edited by P. Michler, Topics in Applied Physics Vol. 90 (Springer-Verlag, Berlin, 2003).
[2] J. P. Reithmaier, G. Sek, A. Löffler, C. Hofmann, S. Kuhn, S. Reitzenstein, L. V. Keldysh, V. D. Kulakovskii, T. L. Reinecke, and A. Forchel, Nature (London) **432**, 197 (2004).
[3] M. Sugisaki, H.-W. Ren, K. Nishi, and Y. Masumoto, Jpn. J. Appl. Phys., Part 1 **41**, 958 (2002).
[4] J. Persson, M. Holm, C. Pryor, D. Hessmann, W. Seifert, L. Samuelson, and M.-E. Pistol, Phys. Rev. B **67**, 035320 (2003).
[5] V. Zwiller, T. Aichele, W. Seifert, J. Persson, and O. Benson, Appl. Phys. Lett. **82**, 1509 (2003).
[6] T. Aichele, V. Zwiller, and O. Benson, New J. Phys. **6**, 90 (2004).
[7] G. J. Beirne, P. Michler, M. Jetter, and H. Schweizer, J. Appl. Phys. **98**, 093522 (2005).
[8] R. Hanbury-Brown and R. Q. Twiss, Nature (London) **178**, 1447 (1956).
[9] V. Zwiller, M. Pistol, D. Hessman, R. Coderstrom, W. Seifert, and L. Samuelson, Phys. Rev. B **59**, 5021 (1999).
[10] E. Dekel, D. V. Regelman, D. Gershoni, E. Ehrenfreund, W. V. Schoenfeld, and P. M. Petroff, Phys. Rev. B **62**, 11038 (2000).
[11] M. Ono, K. Matsuda, T. Saiki, K. Nishi, T. Mukaiyama, and M. Kuwata-Gonokami, Jpn. J. Appl. Phys., Part 2 **38**, L1460 (1999).
[12] Ph. Roussignol, W. Heller, A. Filoramo, and U. Bockelmann, Physica E (Amsterdam) **2**, 588 (1998).
[13] C. Pryor, M.-E. Pistol, and L. Samuelson, Phys. Rev. B **56**, 10404 (1997).

[14] K. L. Janssens, B. Partoens, and F. M. Peeters, Phys. Rev. B **67**, 235325 (2003).
[15] A. Wojs, P. Hawrylak, S. Fafard, and L. Jacak, Phys. Rev. B **54**, 5604 (1996).
[16] M. Paillard, X. Marie, E. Vanelle, T. Amand, V. K. Kalevich, A. R. Kovsh, A. E. Zhukov, and V. M. Ustinov, Appl. Phys. Lett. **76**, 76 (2000).
[17] C. Santori, G. S. Solomon, M. Pelton, and Y. Yamamoto, Phys. Rev. B **65**, 073310 (2002).
[18] D. S. Citrin, Phys. Rev. B **50**, 17655 (1994).
[19] T. Takagahara, Phys. Rev. B **39**, 10206 (1989).
[20] G. Bacher, R. Weigand, J. Seufert, V. D. Kulakovskii, N. A. Gippius, A. Forchel, K. Leonardi, and D. Hommel, Phys. Rev. Lett. **83**, 4417 (1999).
[21] J. Seebeck, T. R. Nielsen, P. Gartner, and F. Jahnke, Phys. Rev. B **71**, 125327 (2005).
[22] N. Baer, C. Gies, J. Wiersig, and F. Jahnke, Eur. Phys. J. B **50**, 411 (2006).